Some General Conditions for Hidden Fermi Surface Nesting

M.-H. Whangbo,* J. Ren, and W. Liang

Department of Chemistry, North Carolina State University, Raleigh, North Carolina 27695-8204

E. Canadell*

Laboratoire de Chimie Théorique, Université de Paris-Sud, 91405 Orsay, France

J.-P. Pouget* and S. Ravy

Laboratoire de Physique des Solides (CNRS LA 2), Université de Paris-Sud, 91405 Orsay, France

J. M. Williams and M. A. Beno

Chemistry and Materials Science Divisions, Argonne National Laboratory, Argonne, Illinois 60439

Received February 21, 1992

Certain low-dimensional metals exhibit charge density wave (CDW) instabilities although their individual Fermi surfaces do not have the nesting responsible for the observed CDW's. This phenomenon is explained in terms of the conept of hidden Fermi surface nesting. In order to find general conditions leading to hidden Fermi surface nesting in low-dimensional systems, we examined the electronic structures of two widely different classes of compounds, i.e., the inorganic transition-metal oxide $Sr_3V_2O_7$ and the organic conducting salts $(BEDT\text{-}TTF)_2ReO_4$ and $(BEDT\text{-}TTF)_4Pt(C_2O_4)_2$.

Introduction

Low-dimensional metals are susceptible to charge density wave (CDW) or spin density wave (SDW) instabilities when their Fermi surfaces are nested.[1,2] However, certain low-dimensional metals with several partially filled bands exhibit CDW instabilities even when their individual Fermi surfaces provide no clue to the nesting responsible for the CDW.[3,4] The hidden Fermi surface nesting responsible for such an observed CDW instability can be found if the individual Fermi surfaces are combined together and then decomposed into nested surfaces by neglecting the surface noncrossings resulting from band hybridizations. This concept of hidden Fermi surface nesting[3,4] (hereafter referred to as hidden nesting) has been crucial in understanding the CDW phenomena of two-dimensional (2D) metals, such as Magnéli phase Mo_4O_{11},[5] purple bronze AMo_6O_{17} (A = K, Na),[3] and monophosphate tungsten bronzes (MPTB's).[6,7] In the present work, we examine some general conditions necessary for the occurrence of a hidden nesting by analyzing the electronic structures of two different classes of low-dimensional metals, i.e., the perovskite-type layer compound $Sr_3V_2O_7$[8] and the organic conducting salts $(BEDT\text{-}TTF)_2ReO_4$[9] and $(BEDT\text{-}TTF)_4Pt(C_2O_4)_2$[10] (BEDT-TTF refers to bis(ethylenedithio)tetrathiafulvalene (**1**)). We calculate the

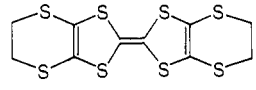

BEDT-TTF

1

band electronic structures of these systems on the basis of the extended Hückel tight-binding (EHTB) method,[11] which has been successful in explaining the CDW instabilities of numerous transition-metal chalcogenides[12] and oxides[3-5,7] as well as organic conducting salts.[13] Computational details of the EHTB method can be found in ref 7.

Hidden Nesting of $Sr_3V_2O_7$

The $Sr_3V_2O_7$ phase consists of isolated V_2O_7 layers of corner-sharing VO_6 octahedra.[8] As schematically shown in Figure 1a, a VO_4 layer (in the coordinate xy plane) is formed from VO_6 octahedra by sharing their equatorial oxygen (O_{eq}) atoms. Then, a V_2O_7 layer is formed from two VO_4 layers by sharing their axial

(1) (a) Lomer, W. M. *Proc. Phys. Soc., London* **1962**, *80*, 489. (b) Overhauser, A. W. *Phys. Rev.* **1962**, *128*, 1437.
(2) (a) Wilson, J. A.; DiSalvo, F. J.; Mahajan, S. *Adv. Phys.* **1975**, *24*, 117. (b) DiSalvo, F. J. *Electron-Phonon Interactions and Phase Transitions*; Plenum: New York, 1977; p 107.
(3) Whangbo, M.-H.; Canadell, E.; Foury, P.; Pouget, J. P. *Science* **1991**, *252*, 96.
(4) Canadell, E.; Whangbo, M.-H. *Chem. Rev.* **1991**, *91*, 965.
(5) Canadell, E.; Whangbo, M.-H.; Schlenker, C.; Escribe-Filippini, C. *Inorg. Chem.* **1989**, *28*, 1466 and references cited therein.
(6) (a) Foury, P.; Pouget, J. P.; Wang, E.; Greenblatt, M. *Europhys. Lett.* **1991**, *16*, 485. (b) Wang, E.; Greenblatt, M.; Rachidi, I E.-I.; Canadell, E.; Whangbo, M.-H.; Vadlamannati, S. *Phys. Rev. B.* **1989**, *39*, 12969.
(7) Canadell, E.; Whangbo, M.-H. *Phys. Rev. B* **1991**, *43*, 1894.
(8) Suzuki, N.; Noritake, T.; Yamamoto, N.; Hioki, T. *Mater. Res. Bull.* **1991**, *26*, 1.
(9) (a) Parkin, S. S. P.; Engler, E. M.; Schumaker, R. R.; Lagier, R.; Lee, V. Y.; Scott, J. C.; Green, R. *Phys. Rev. Lett.* **1983**, *50*, 270. (b) Whangbo, M.-H.; Beno, M. A.; Leung, P. C. W.; Emge, T. J.; Wang, H. H.; Williams, J. M. *Solid State Commun.* **1986**, *59*, 813.
(10) Gärtner, S.; Heinen, I.; Schweitzer, D.; Nuber, B.; Keller, H. J. *Synth. Met.* **1989**, *31*, 199.
(11) Whangbo, M.-H.; Hoffmann, R. *J. Am. Chem. Soc.* **1978**, *100*, 6093.
(12) (a) Canadell, E.; Rachidi, I. E.-I.; Pouget, J. P.; Gressier, P.; Meerschaut, A.; Rouxel, J.; Jung, D.; M. Evain, M.; Whangbo, M.-H. *Inorg. Chem.* **1990**, *29*, 1401. (b) Gressier, P.; Whangbo, M.-H.; Meerschaut, A.; Rouxel, J. *Inorg. Chem.* **1984**, *23*, 1221. (c) Whangbo, M.-H.; Gressier, P. *Inorg. Chem.* **1984**, *23*, 1305. (d) Whangbo, M.-H.; DiSalvo, F. J.; Fleming, R. M. *Phys. Rev. B* **1982**, *26*, 687. (e) Canadell, E.; Whangbo, M.-H. *J. Am. Chem. Soc.* **1988**, *110*, 104.
(13) For a review, see: Williams, J. M.; Wang, H. H.; Emge, T. J.; Geiser, U.; Beno, M. A.; Leung, P. C. W.; Carlson, K. D.; Thorn, R. J.; Schultz, A. J.; Whangbo, M.-H. *Prog. Inorg. Chem.* **1985**, *33*, 183.

0020-1669/92/1331-4169$03.00/0

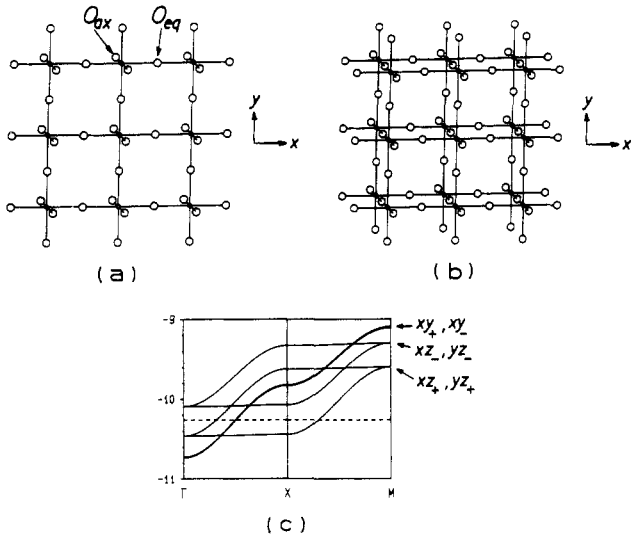

Figure 1. (a) Perspective view of a VO_4 layer. (b) Perspective view of a V_2O_7 layer present in $Sr_3V_2O_7$. (c) Dispersion relations of the t_{2g}-block bands calculated for $Sr_3V_2O_7$, where the Fermi level is represented by the dashed line. $\Gamma = (0, 0)$, $X = (a^*/2, 0)$, and $Y = (0, b^*/2)$.

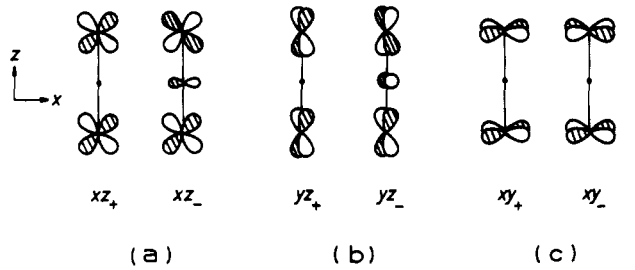

Figure 2. Orbital patterns of the V–O_{ax}–V linkage contributing to the t_{2g}-block bands of Figure 1c: (a) xz_+ and xz_-; (b) yz_+ and yz_-; (c) xy_+ and xy_-.

oxygen (O_{ax}) atoms, as shown in Figure 1b. The Sr^{2+} cations of $Sr_3V_2O_7$ are found in the 12-coordinate sites within each V_2O_7 layer and also in the 9-coordinate sites between adjacent V_2O_7 layers.[8] The dispersion relations calculated for the t_{2g}-block bands of $Sr_3V_2O_7$ are shown in Figure 1c. The orbitals of each V–O_{ax}–V linkage (along the coordinate z axis) leading to the six t_{2g}-block bands are schematically represented in Figure 2. The xz_+ and yz_+ bands are lower in energy than the xz_- and yz_- bands because they do not have p-orbital contributions from the bridging O_{ax} atoms.[4] The xy_+ and xy_- bands are practically degenerate because the bridging O_{ax} atom p orbitals cannot interact with the xy orbitals due to their δ symmetry along the V–O_{ax}–V axis.

With the formal oxidation state of V^{4+}, there are two electrons to fill the t_{2g}-block bands of Figure 1c, thereby leading to four partially filled bands. The Fermi surfaces associated with these bands are shown in Figure 3a–d, where the occupied wave vector regions are indicated by shading. The xy_+ and xy_- bands give rise to circular Fermi surfaces (Figure 3a,b), and the xz_+ and yz_+ bands to squarelike Fermi surfaces (Figure 3c,d). Taken separately, the squarelike surfaces each signify a 2D metallic character. However, when combined together as shown in Figure 3e, these two surfaces are decomposed into two sets of nearly parallel, i.e., one-dimensional (1D), Fermi surfaces. The set parallel to $\Gamma \rightarrow Y$ originates from the xz_+ band, which is dispersive only along $\Gamma \rightarrow X$, and the other set parallel to $\Gamma \rightarrow X$ arises from the yz_+ band, which is dispersive only along $\Gamma \rightarrow Y$. According to these hidden 1D Fermi surfaces, a V_2O_7 layer can be regarded as made up of two orthogonal sets of "chains". For example, along $\Gamma \rightarrow Y$, the metal xz orbitals do not interact through the V–O_{eq}–V bridges because of their δ symmetry along that direction. Thus, as far as the xz_+ and xz_- bands are concerned, each V_2O_7 layer is made up of noninteracting xz orbitals containing chains

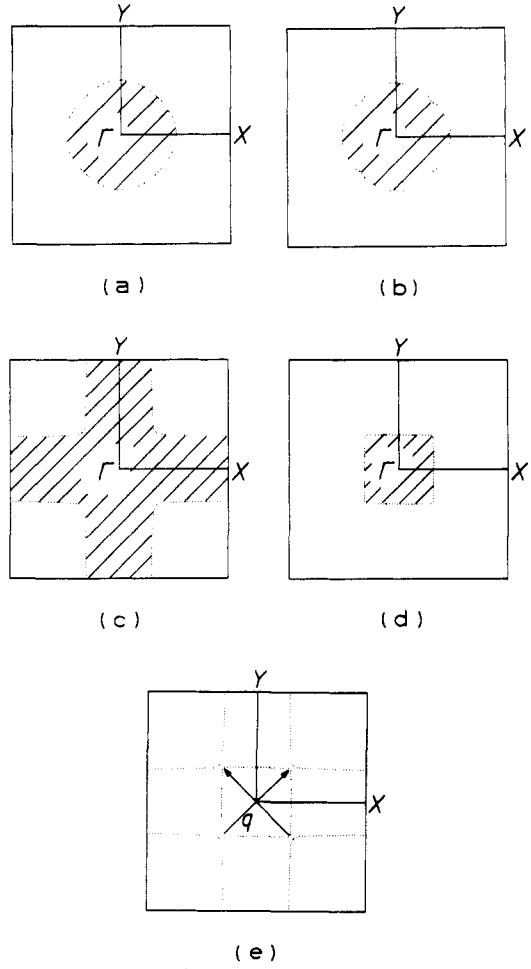

Figure 3. Fermi surfaces associated with the t_{2g}-block bands of Figure 1c: (a, b) from the xy_+ and xy_- bands; (c, d) from the xz_+ and yz_+ bands. The hidden nesting is illustrated in (e).

parallel to $\Gamma \rightarrow X$. Likewise, for the yz_+ and yz_- bands, each layer is made up of noninteracting yz orbitals containing chains parallel to $\Gamma \rightarrow Y$.

The two hidden 1D surfaces of Figure 3e are well nested by a single common nesting vector $q \simeq (1/3, \pm 1/3)$, which links the crossing points of the hidden surfaces, as previously found for Mo_4O_{11},[5] AMo_6O_{17},[3] and the MPTB's.[6] Such a nesting would open an energy gap on most of the Fermi surfaces of Figure 3c,d and can lead to a large gain of electronic energy. With decreasing temperature, the resistivity of $Sr_3V_2O_7$ measured for polycrystalline samples decreases almost linearly[8] and shows a slower decrease below ~100 K. It would be interesting to examine whether single crystals of $Sr_3V_2O_7$ exhibit a CDW or an SDW instability (associated with the common nesting vector of the hidden surfaces) in this low-temperature range. However, a metal–insulator transition is not expected because the quasi-circular Fermi surfaces (Figure 3a,b) will not be affected by the nesting.

Hidden Nesting of $(BEDT\text{-}TTF)_2ReO_4$ and $(BEDT\text{-}TTF)_4Pt(C_2O_4)_2$

In most 2:1 $(BEDT\text{-}TTF)_2X$ salts of the organic donor molecule BEDT-TTF with a mononegative anion X^-,[13] the layers of the donor molecules alternate with layers of the anions along one crystallographic direction. Figure 4a shows a perspective view of the donor-molecule layer (in the crystallographic ab plane) of $(BEDT\text{-}TTF)_2ReO_4$, where the sulfur and carbon atoms are represented by large and small circles, respectively. The donor molecules are inclined with respect to the donor-molecule plane such that each donor molecule of Figure 4a is viewed approxi-

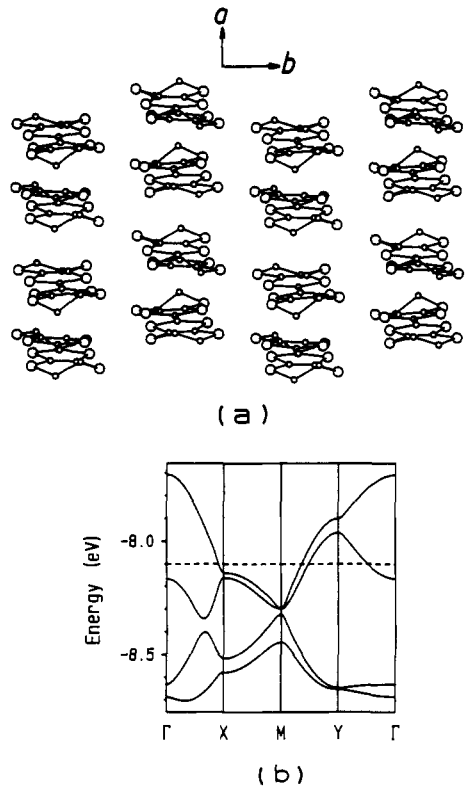

Figure 4. (a) Perspective view of a donor-molecule layer of (BEDT-TTF)$_2$ReO$_4$. The large and small circles represent the sulfur and carbon atoms of BEDT-TTF, respectively, and the hydrogen atoms are not shown for simplicity. Each donor molecule is viewed roughly along the direction of its central C=C bond. (b) Dispersion relations of the four highest occupied bands calculated for a single donor-molecule layer of (BEDT-TTF)$_2$ReO$_4$ on the basis of its crystal structure determined at 125 K, where the Fermi level is represented by the dashed line. $\Gamma = (0, 0)$, $X = (a^*/2, 0)$, $M = (a^*/2, b^*/2)$, and $Y = (0, b^*/2)$.

mately along the direction of its central C=C bond (see **1**). The donor-molecule layer of (BEDT-TTF)$_2$ReO$_4$ consists of donor-molecule stacks which run along the a-axis direction. A unit cell of the donor-molecule layer contains two donor-molecule stacks, and that of each donor-molecule stack contains two donor molecules. Thus, a unit cell of the donor-molecule layer of (BEDT-TTF)$_2$ReO$_4$ contains four donor molecules.

In a 2:1 (BEDT-TTF)$_2$X salt such as (BEDT-TTF)$_2$ReO$_4$, the magnitudes of the intra and interstack interactions between the donor molecules depend sensitively on the short S···S contacts between the donor molecules.[13] Thus, local displacements of the donor molecules (e.g., slight rotations of BEDT-TTF around the central C=C bond and around the axes perpendicular to this bond, slight movements of BEDT-TTF perpendicular to the stacking direction, etc.) can change the relative magnitudes of the intra- and interstack interactions, thereby ultimately affecting the dimensionality of the electrical conductivities of the donor-molecule salt.

Figure 4b shows the dispersion relations of the four highest occupied bands [i.e., those derived mainly from the highest occupied molecular orbitals (HOMO's) of the donor molecules] of a single donor-molecule layer of (BEDT-TTF)$_2$ReO$_4$ calculated on the basis of the crystal structure determined at 125 K.[9b] With the ReO$_4^-$ anions, the average oxidation state of the donor molecule in (BEDT-TTF)$_2$ReO$_4$ is BEDT-TTF$^{0.5+}$. Thus, there are six electrons to fill the four bands of Figure 4b, so that the Fermi level (shown by the dashed line) cuts the third and fourth bands from the bottom. The third band leads to the hole surface of Figure 5a, and the fourth band to the electron surface of Figure 5b.[9b] The hole surface is a closed loop and is 2D in character, while the electron surface is open and is 1D in character.

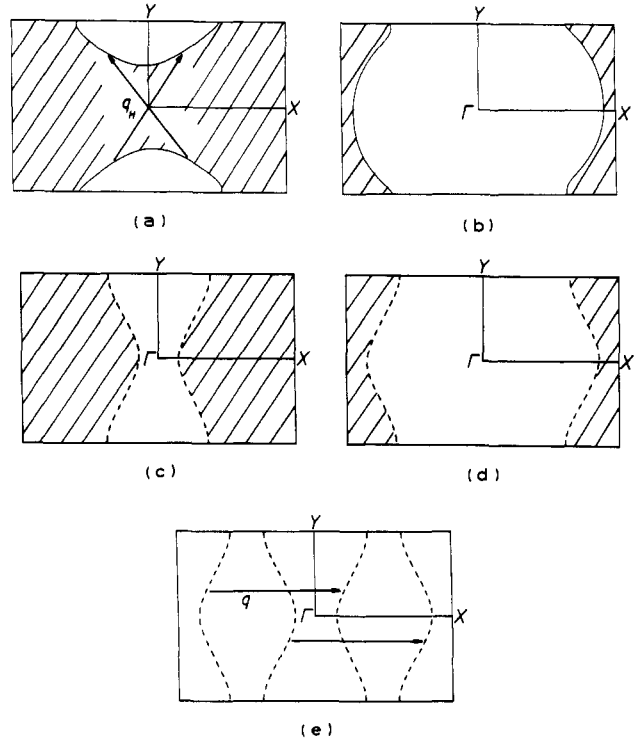

Figure 5. Fermi surfaces calculated for the 125 K structure of (BEDT-TTF)$_2$ReO$_4$ and expected hidden surfaces: (a) calculated hole surface; (b) calculated electron surface; (c) expected hidden hole surface; (d) expected hidden electron surface. The nesting expected from the hidden Fermi surfaces is shown in (e).

(BEDT-TTF)$_2$ReO$_4$ is an anisotropic metal down to 77 K, at which it undergoes a strong first-order structural transition[14] stabilizing a ($^1/_2$, 0, $^1/_2$) structural modulation, which leads to a semiconducting state. Below 77 K, the donor stack periodicity is doubled,[15] so that the 77 K transition could result from a Peierls transition expected for a 1D metal with a half-filled band. However, the Fermi surfaces of (BEDT-TTF)$_2$ReO$_4$ do not exhibit a $2k_f$ nesting wave vector of $0.5a^*$, which is necessary for explaining the phase transition by a simple Peierls mechanism. Therefore, it is interesting to examine whether or not the Fermi surfaces of (BEDT-TTF)$_2$ReO$_4$, when slightly perturbed, possess a hidden nesting wave vector of $0.5a^*$.

The 2D character of the hole surface arises from the fact that the third band of Figure 4b is dispersive along the intrastack ($\Gamma \rightarrow X$ and $M \rightarrow Y$) and interstack ($\Gamma \rightarrow Y$ and $X \rightarrow M$) directions. If the interstack hopping interactions become sufficiently weak by appropriate secondary displacements of donor molecules (e.g., the local displacements of the donor molecules already mentioned), it is possible that the energy of the third band at Γ is pushed above the Fermi level. Then the Fermi surface of this band becomes 1D, as illustrated in Figure 5c. In this figure, the occupied wave vector region is taken to be smaller than that of Figure 5a. The total occupied wave vector area of the hole and electron surfaces should remain constant, so that the decrease in the occupied region of the hole surface (from Figure 5a to Figure 5c) should be compensated by a corresponding increase in the occupied region of the electron surface (i.e., from Figure 5b and Figure 5d). The Fermi surfaces of Figure 5c,d are the hidden surfaces expected for (BEDT-TTF)$_2$ReO$_4$ when its interstack interactions become weak. As illustrated in Figure 5e, the hidden surfaces lead to an interband nesting wave vector of $0.5a^*$, consistent with that observed in (BEDT-TTF)$_2$ReO$_4$ below 77 K.

If the energy required to reduce the interstack hopping interactions is more than compensated by the electronic energy

(14) Ravy, S.; Moret, R.; Pouget, J. P.; Comes, R., Parkin, S. S. P. *Phys. Rev. B* **1986**, *33*, 2049.
(15) Ravy, S.; Moret, R.; Pouget, J. P.; Comes, R. *Synth. Met.* **1987**, *19*, 237.

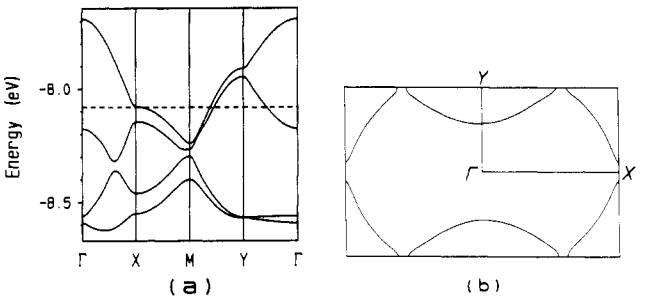

Figure 6. (a) Dispersion relations of the four highest occupied bands calculated for the room-temperature structure of (BEDT-TTF)$_2$ReO$_4$. (b) Fermi surfaces associated with the partially filled bands of part a.

gain resulting from the CDW formation associated with a hidden nesting, the salt would undergo a metal–insulator transition and stabilize the hidden nesting wave vector. In this respect, it is interesting to remark that the energy of holes near Γ (~0.06 eV; see Figure 4b) is comparable to the band gap (~0.05 eV)[9a] opened by the metal–insulator transition of (BEDT-TTF)$_2$ReO$_4$. Such a mechanism is more likely to occur if a weakening of interstack interactions occurs upon temperature lowering. This seems to be the case for (BEDT-TTF)$_2$ReO$_4$: parts a and b, respectively, of Figure 6 show the dispersion relations and the Fermi surfaces calculated for (BEDT-TTF)$_2$ReO$_4$ on the basis of its room-temperature structure.[9b] Note that both the hole and the electron surfaces possess a 2D character at room tempeature. The temperature lowering from room temperature to 125 K elongates the hole surface along the Γ → *X* direction (Figure 6b vs Figure 5a) and converts the character of the electron surface from 2D to 1D. Thus as the temperature is lowered from room temperature to 125 K, (BEDT-TTF)$_2$ReO$_4$ increases in 1D character, and this trend is expected to persist below 125 K.[16]

It should be remarked that the first-order character of the phase transition of (BEDT-TTF)$_2$ReO$_4$ is unusual among the CDW materials, which generally exhibit a second-order Peierls transition with a sizable regime of pretransitional fluctuations.[17] Due to a strong first-order nature of the 77 K phase transition, pretransitional fluctuations associated with the hidden nesting are not observed for (BEDT-TTF)$_2$ReO$_4$.[14] This first-order phase transition requires a strong coupling between a primary order parameter ψ, describing the modulation of the donor stack, and a secondary distortion ϕ (e.g., the contraction of the *a*-axis length[16]), related to some secondary displacements of the donor molecules which weaken the interstack hopping interactions, thereby providing the hidden nesting. An argument is given in the Appendix within the framework of a phenomenological Landau theory. The 77 K CDW phase transition of (BEDT-TTF)$_2$ReO$_4$ vanishes under a pressure greater than ~4 kbar, which is due probably to an increase in the interstack hopping interactions. With the restoration of a metallic state, this salt becomes a superconductor.[9a]

The donor layers[10] of (BEDT-TTF)$_4$Pt(C$_2$O$_4$)$_2$ are quite similar in structure to those of (BEDT-TTF)$_2$ReO$_4$. Consequently, the band dispersion relations and the Fermi surfaces of (BEDT-TTF)$_4$Pt(C$_2$O$_4$)$_2$ calculated for its room-temperature structure are almost identical to those of (BEDT-TTF)$_2$ReO$_4$ (at 125 K) shown in Figures 4b and 5a,b (hence not shown). However, (BEDT-TTF)$_4$Pt(C$_2$O$_4$)$_2$ seems to undergo two phase transitions as the temperature is lowered, i.e., a metal–metal transition at 200 K and a metal–insulator transition at 60–80 K (sample dependent).[10] The thermopower measurements show that (BEDT-TTF)$_4$Pt(C$_2$O$_4$)$_2$ has both electron and hole carriers and the 200 K transition removes hole carriers primarily.[10] The latter is due probably to a partial nesting in the hole surface (see Figure 5a). It would be interesting to examine whether or not the 200 K and the 60–80 K phase transitions of (BEDT-TTF)$_4$Pt(C$_2$O$_4$)$_2$ are second order in nature. It would be also interesting to determine whether the crystal structure of (BEDT-TTF)$_4$Pt(C$_2$O$_4$)$_2$ below 60 K shows a doubling of the donor stack periodicity. For this will show whether or not the overall result of the two consecutive (second-order) phase transitions in (BEDT-TTF)$_4$Pt(C$_2$O$_4$)$_2$ is formally equivalent to that of a hypothetical first-order phase transition associated with the hidden nesting. A metal–insulator Peierls transition achieved by a two-step process was previously reported for Cs[Pd(dmit)$_2$]$_2$.[19]

It is interesting to notice that, although the electronic structures of the (BEDT-TTF)$_2$ReO$_4$ and (BEDT-TTF)$_4$Pt(C$_2$O$_4$)$_2$ salts are virtually identical, the two salts undergo quite different sequences of phase transitions. Certainly, this is caused by the difference in their lattice properties, since the donor···anion contact interactions involve anions of different shapes (i.e., tetrahedral ReO$_4^-$ and planar Pt(C$_2$O$_4$)$_2^{2-}$ anions). This could influence the symmetry and the strength of the coupling between the primary and the secondary order parameters (see Appendix). It would be important to increase the interstack hopping interactions of (BEDT-TTF)$_4$Pt(C$_2$O$_4$)$_2$ by applying pressure, to see whether a superconducting state may be stabilized, as in the case of (BEDT-TTF)$_2$ReO$_4$.[20]

Discussion and Concluding Remarks

The inorganic materials exhibiting hidden nested Fermi surfaces, i.e., purple bronze AMo$_6$O$_{17}$ (A = K, Na, Tl), Magnéli phase Mo$_4$O$_{11}$, the MPTB's, and Sr$_3$V$_2$O$_7$, have a common structural feature that their metal–oxygen layers made up of MO$_6$ octahedra (M = Mo, W, V) possess partially filled t_{2g}-blocked bands. The three t_{2g}-block orbitals of each MO$_6$ octahedron are contained in three mutually orthogonal planes and act as δ orbitals toward the M–O axes perpendicular to these planes. Therefore, for certain or all t_{2g} orbitals (e.g., the *xz* and *yz* orbitals of Sr$_3$V$_2$O$_7$), the metal–oxygen layers can be regarded as made up of noninteracting t_{2g}-orbital-containing chains. The t_{2g} orbitals of an MO$_6$ octahedron are orthogonal to one another, and direct metal–metal interactions between adjacent metal centers are negligible due to the corner-sharing nature of the metal–oxygen layers. Therefore, hybridization among the different t_{2g}-block bands is not strong. It is natural that the AMo$_6$O$_{17}$, Mo$_4$O$_{11}$, MPTB, and Sr$_3$V$_2$O$_7$ systems exhibit hidden quasi-1D Fermi surfaces, which are well nested, thus allowing for the onset of CDW or SDW instabilities.

Organic salts are essentially molecular crystals, and thus bonding between donor molecules and that between donor molecules and anions are not strong. Therefore, when the temperature is lowered, donor molecules may undergo slight displacements to adjust to the ensuing decrease in the unit cell

(16) In particular, the *a*-axis length is observed to continue to decrease with the same rate as the temperature is lowered below 125 K. See ref 14 and: Williams, J. M.; Beno, M. A.; Wang, H.-H.; Reed, P. E.; Azevedo, L. J.; Schirber, J. E. *Inorg. Chem.* **1984**, *23*, 1792.

(17) For detailed applications, see: Moret, R.; Pouget, J. P. In *Crystal Chemistry and Properties of Materials with Quasi-One-Dimensional Structures*; Rouxel, J., Ed.; Reidel: Dordrecht, The Netherlands, 1986; p 87.

(18) Imry, Y. *J. Phys. C: Solid State Phys.* **1975**, *8*, 567.

(19) Underhill, A. E.; Clark, R. A.; Marsden, I.; Allan, M.; Friend, R. H.; Tajima, H.; Naito, T.; Tamura, T.; Kuroda, H.; Kobayashi, A.; Kobayashi, H.; Canadell, E.; Ravy, S.; Pouget, J. P. *J. Phys.: Condens. Matter* **1991**, *3*, 933.

(20) After the completion of our work, a new metallic salt (BEDT-TTF)$_4$Cu(C$_2$O$_4$)$_2$ was reported.[21,22] When the temperature is lowered, it exhibits small resistivity anomalies at 262 and 160 K before undergoing a metal–insulator transition at 65 K.[21] The crystal structure[22] and the electronic structure[23] of this salt are very similar to those of (BEDT-TTF)$_4$Pt(C$_2$O$_4$)$_2$.

(21) Wang, P.; Bandow, S.; Maruyama, Y.; Wang, X.; Zhu, D. *Synth. Met.* **1991**, *44*, 147.

(22) Qian, M.; Rudert, R.; Luger, P.; Ge, C.; Wang, X. *Acta Crystallogr.* **1991**, *C47*, 2358.

(23) Martin, J. D.; Canadell, E. Unpublished results.

volume. This could change the extent of the 1D or 2D character of the Fermi surfaces. Therefore, recognition of a hidden nesting on the basis of the Fermi surfaces calculated for room-temperature crystal structures may become less obvious for organic salts than for inorganic extended systems. In addition, the partially filled bands of most organic donor salts are all derived from the HOMO of each donor molecule, which is a π orbital. That is, each donor molecule contributes one orbital to the partially filled bands in contrast to the case of the MO_6 octahedra of the metal–oxygen layers of the AMo_6O_{17}, Mo_4O_{11}, MPTB, and $Sr_3V_2O_7$ systems, in which each MO_6 octahedron contributes three orthogonal orbitals to the partially filled bands. Therefore, the origin of the hidden nesting in the organic salts (BEDT-TTF)$_2$ReO$_4$ and (BEDT-TTF)$_4$Pt(C$_2$O$_4$)$_2$ is qualitatively different from that found for the AMo_6O_{17}, Mo_4O_{11}, MPTB, and $Sr_3V_2O_7$ systems. In the organic salts, the hidden nesting occurs via a secondary distortion which restores a quasi-1D Fermi surface exhibiting a conventional Peierls instability. In the inorganic oxides, the hidden nesting removes the band hybridization and stabilizes CDW's with wave vectors which link the crossing points of overlapping quasi-1D Fermi surfaces.

Nevertheless, the organic salts and the inorganic oxides examined in the present work have a common structural feature that each system can be considered as made up of chains (e.g., the t_{2g}-orbital-containing chains in the inorganic oxides and the donor stacks in the organic salts). They also possess the common electronic features that each system has several partially filled bands and that the hidden nesting is seen only if the individual Fermi surfaces are combined together as a whole. Occurrence of a CDW instability associated with a hidden nesting is possible when the electronic energy gain resulting from the CDW formation dominates over the energy required for reducing the extent of "interchain" interactions.

Acknowledgment. This work was supported by the U.S. Department of Energy, Office of Basic Energy Sciences, under Grant DE-FG05-86ER45259 and Contract W-31-109-ENG-38, and also by NATO, Scientific Affairs Division.

Appendix

The free energy of the two order parameters Ψ and Φ discussed in the text can be written as

$$F(\Psi,\Phi) = F_1(\Psi) + F_2(\Phi) + F_3(\Psi,\Phi) \quad (1)$$

Here F_1 is the CDW-related free energy (associated with the Fermi surface nesting) describing the conventional second-order Peierls transition. F_2 is the strain energy caused by a secondary distortion Φ. F_3 is the additional gain of CDW free energy due to the secondary distortion. At the lowest orders of Ψ and Φ

$$F_1 = (A/2)\Psi^2 + (B/4)\Psi^4 \quad (2)$$

where A becomes negative below a critical temperature T_c and $B > 0$, and

$$F_2 = (D/2)\Phi^2 + (E/4)\Phi^4 \quad (3)$$

with $D > 0$ and $E > 0$. Depending upon the symmetry of the secondary distortion, F_3 is written at the lowest order either as

$$F_3 = -C\Phi\Psi^2 \quad (4)$$

or as

$$F_3 = -(C/2)\Phi^2\Psi^2 \quad (5)$$

with $C > 0$. The energy term of eq 4 vanishes when the interstack hopping interactions are an odd function of Φ.

The values of the order parameters satisfy the minimization conditions $\delta F/\delta\Psi = 0$ and $\delta F/\delta\Phi = 0$. Thus, when the leading term of F_3 is given by eq 4, the free energy is rewritten as

$$F = (A/2)\Psi^2 + (B/4 - C^2/2D)\Psi^4 \quad (6)$$

by neglecting the second term of eq 3. Equation 6 predicts a second-order phase transition at a critical temperature T_c if $BD > 2C^2$ but a first-order transition if $BD < 2C^2$ at a critical temperature higher than T_c.[17] When the leading term of F_3 is given by eq 5, a similar calculation[18,19] predicts two successive second-order phase transitions (the upper one being at T_c) if $BE > C^2$ but a first-order phase transition (at a critical temperature higher than T_c) if $BE < C^2$. A weak coupling (i.e., small C) could explain the two successive phase transitions of (BEDT-TTF)$_4$Pt(C$_2$O$_4$)$_2$.[10] This situation is also encountered in the CDW material Cs[Pd(dmit)$_2$]$_2$.[19] Regardless of the Φ dependence of F_3, a large coupling (i.e., large C) leads to a first-order transition, as observed for (BEDT-TTF)$_2$ReO$_4$. In the case of large coupling, it should be remarked that even if F_1, though being close to a CDW instability, does not exhibit a singular behavior at a finite value of T_c, a Peierls ground state can be stabilized on a finite temperature range after a first-order phase transition.